

## Electronic structure of the substitutional nitrogen $NN_1$ pair in GaP from photoluminescence excitation and Zeeman spectroscopy

Q. X. Zhao and B. Monemar

*Department of Physics and Measurement Technology, Linköping University, S-581 83 Linköping, Sweden*

(Received 3 December 1987)

Novel photoluminescence (PL) data are presented for the nearest-neighbor substitutional  $NN_1$  ( $N_P-N_P$ ) pair defect in GaP, with a bound exciton (BE) at 2.185 eV at 2 K. The zero-field electronic line spectrum of this BE is accurately determined via photoluminescence excitation (PLE) spectra, which give the relative oscillator strengths of the six PL lines resolved. In addition Zeeman data are obtained for magnetic fields up to 7 T, including the full angular dependence. An explicit expression is derived for the evaluation of the zero-field splitting of the BE substates, in terms of the electron-hole ( $e-h$ ) exchange parameter  $a$  and the crystal-field parameters  $D$  and  $E$ . Computer-simulated relative oscillator strengths obtained with a simple basis set of spinlike electrons and  $J = \frac{3}{2}$  holes show a good agreement with the observed relative intensities of the electronic BE lines in PLE spectra. The Zeeman data were analyzed with a complete Hamiltonian including the zero-field perturbations. The evaluated parameter values are  $a = 0.585$  meV,  $D = 0.20$  meV,  $E = 0.095$  meV,  $g_e = 1.85$ ,  $K = 1.21$ , and  $L = -0.05$ , with conventional notations. The zero-field parameters  $a$ ,  $D$ , and  $E$  in particular differ markedly from earlier less accurate data, while the magnetic parameters  $g_e$ ,  $K$ , and  $L$  are in agreement with earlier estimates, although more accurate. The data confirm a  $C_{2v}$  symmetry of the defect, as was previously deduced from uniaxial stress perturbations.

### I. INTRODUCTION

Since the first report in literature on the identification of bound excitons (BE's) associated with substitutional nitrogen in GaP more than two decades ago,<sup>1</sup> there have been numerous publications on this subject.<sup>1-9</sup> One reason for this great interest is the strong luminescence associated with such "isoelectronic" defects in GaP, which has found practical applications in light-emitting devices in the green and yellow spectral region.<sup>10</sup> The electronic structure of the BE for isolated substitutional  $N_P$  was investigated early.<sup>1,11-13</sup> The substitutional pair defects  $N_P-N_P$ , which appear at high N doping levels, have a more complicated electronic structure.<sup>1</sup> Several papers on the electronic structure of these nearest-neighbor (NN) pairs have been published during the last decade, advancing understanding.<sup>5,7-9,14,15</sup>

It seems clear that for both the isolated  $N_P$  and for NN pairs the local potential is strongly electron attractive, so that an electron is bound first in a quite localized potential.<sup>16</sup> The hole in the BE is localized in the Coulomb potential of the bound electron, and behaves as a shallow acceptor hole.<sup>5</sup> This is a typical example of the so-called Hopfield-Thomas-Lynch (HTL) model,<sup>17</sup> experimentally proved for NN pairs by photoluminescence excitation (PLE) spectra.<sup>5</sup> The theoretical calculation of the energy position of the corresponding BE lines (or the energy of the primary bound electron) is a very difficult task (a genuine deep-level problem), which has also attracted recent interest.<sup>14,15</sup>

Experimental investigations of the electronic structure of NN-pair lines have concentrated on photoluminescence (PL) spectra at various temperatures,<sup>7</sup> dye-laser-

excited PLE spectra for excited single-particle hole states,<sup>5</sup> and perturbation spectroscopy by an external stress field (hydrostatic as well as uniaxial).<sup>8,9</sup> Zeeman data were only published in an early preliminary report, without a detailed analysis.<sup>1</sup> The zero-field electronic structure of NN pairs is understood in its major features from an analysis of zero-field PL spectra at various temperatures.<sup>1,7</sup> The analysis in Ref. 7 was incomplete, however, in the sense that the nondiagonal contributions to the local strain field were treated by a perturbation approach. As a consequence, only a very approximate description of the splitting patterns and the relative oscillator strengths of the zero-field BE lines for each NN pair was provided. Furthermore, experimental data on oscillator strengths were estimated from thermalization of PL spectra only.<sup>7</sup>

In this work we have obtained detailed PLE spectra of the no-phonon lines of the  $NN_1$  BE, for the first time, using tunable dye-laser spectroscopy. These data allow a determination of the relative oscillator strengths of the zero-field components of the BE. Also, we have made a more complete analysis of the zero-field energy spectra, compared to the previous work. A simultaneous diagonalization of the entire zero-field perturbation matrix [electron-hole ( $e-h$ ) exchange interaction plus the local strain field] has been done, with a suitable basis set for the BE wave functions, and without resort to perturbation theory for the evaluation of nondiagonal elements of the local strain tensor. This diagonalization procedure also gives the perturbed wave functions for any BE line, from which oscillator strengths could be computed, for direct comparison with experimental data. In this work we have also attempted a detailed Zeeman study of the

NN<sub>1</sub>-pair bound-exciton lines in GaP, for the first time. An accurate evaluation of the BE Hamiltonian could be done for the NN<sub>1</sub> BE. It is firmly concluded that this pair has C<sub>2v</sub> symmetry, consistent with a nearest-neighbor ⟨110⟩-oriented pair as the identity of NN<sub>1</sub>.

Section II contains a description of the samples and the experimental conditions. Section III summarizes briefly the formalism for the description of the zero-field spectra and the Zeeman data, in terms of a perturbation Hamiltonian for the BE states. Sections IV and V contain the experimental data, and the results of a computer evaluation of these data, simulating the observed spectra. Section VI summarizes the major conclusions from this work.

## II. SAMPLES AND EXPERIMENTAL PROCEDURE

The N-doped GaP samples used in this study were from liquid-phase-epitaxial (LPE) wafers, obtained from Showa Denko KK, Japan, and from the University of Manchester. They were nitrogen doped during growth to a total concentration varying between 10<sup>17</sup> and 10<sup>18</sup> cm<sup>-3</sup>. The thickness of the epilayer was 20–40 μm, and the substrate was nominally undoped bulk liquid-encapsulated Czochralski-grown (LEC) material.

Photoluminescence measurements were done in an exchange-gas-type He cryostat, where the temperature could be varied from 1.8 K up to room temperature. The excitation source was either an Ar<sup>+</sup> laser (5145 Å) or a cw dye laser (Coumarin-540 dye), the latter being used for photoluminescence excitation (PLE) spectra.

Zeeman data were obtained at 1.8 and 4.2 K in the Voigt configuration at magnetic fields up to 7 T. A Jobin-Yvon THR-1500 high-resolution monochromator was used on the detection side. An attempt was made to record Zeeman data in photoluminescence excitation spectra on samples of somewhat higher doping, but the intensities were too weak to allow meaningful data. The limitation of the accuracy in the present Zeeman data is the natural linewidth of the BE lines for the NN pairs, in our best examples, about 0.10 meV.

## III. THE ENERGY SPECTRUM FOR A BOUND EXCITON ASSOCIATED WITH A NITROGEN PAIR DEFECT

### A. The perturbation Hamiltonian at zero field

Without external fields the perturbation Hamiltonian for a bound exciton at a neutral (“isoelectronic”) defect in GaP contains two major terms:

$$H^{\text{BE}} = H_{\text{ex}} + H_{\text{LCF}}, \quad (1)$$

where  $H_{\text{ex}}$  is the electron-hole ( $e$ - $h$ ) exchange interaction represented by

$$H_{\text{ex}} = -a \mathbf{J}_h \cdot \mathbf{S}_e - b (J_{hx}^3 S_{ex} + J_{hy}^3 S_{ey} + J_{hz}^3 S_{ez}). \quad (2)$$

Here,  $\mathbf{J}_h$  is the total angular momentum of the hole, and  $\mathbf{S}_e$  is the same quantity for the electron (usually spinlike);  $x, y, z$  refer to cubic axes of GaP. The second term in Eq. (2) represents the anisotropic contribution to  $e$ - $h$  ex-

change, and can usually be neglected compared to the first (isotropic) part.

The term  $H_{\text{LCF}}$  represents the perturbation on the BE from the local crystal field at the defect. This term can, in general, be represented by<sup>16,18</sup>

$$H_{\text{LCF}} = -A_2^0 [J_{hz}^2 - \frac{1}{3} J_h (J_h + 1)] - A_2^2 (J_{hx}^2 - J_{hy}^2), \quad (3)$$

where it is assumed that only the hole is affected by the local low-symmetry crystal field, since the electron is assumed to be spinlike and therefore has no orbital angular momentum.<sup>16</sup> In C<sub>3v</sub> symmetry  $A_2^0 = 0$  while  $A_2^2 = 0$ , while in lower symmetries both terms are nonzero. Shifting to the more convenient notation  $A_2^0 \equiv D$ ,  $A_2^2 \equiv E$ , and changing to local defect coordinates, the zero-field perturbation Hamiltonian to be used for a discussion of the electronic structure of BE's associated with NN pairs in GaP can be summarized as follows:

$$H^{\text{BE}} = -a \mathbf{S}_e \cdot \mathbf{J}_h - D [J_{hz}^2 - \frac{1}{3} J_h (J_h + 1)] - E (J_{hx}^2 - J_{hy}^2). \quad (4)$$

Here,  $z', y', z'$  denotes the principal set of axes for the local crystal field associated with the complex defect. Equation (4) is sufficient for a description of defects with C<sub>2v</sub> symmetry (or higher); for the case of lower symmetry the inclusion of additional nondiagonal terms in the tensor describing the local-crystal-field splitting may be necessary.

### B. The Zeeman Hamiltonian

The perturbation Hamiltonian  $H^{\text{BE}}$  used in evaluating the Zeeman data has the form

$$H^{\text{BE}} = H_{\text{ex}} + H_{\text{LCF}} + H_{\text{LZ}} + H_{\text{QZ}}, \quad (5)$$

where the first term  $H_{\text{ex}}$  is identical to Eq. (2), and the  $H_{\text{LCF}}$  term is given by Eq. (3). The linear Zeeman term  $H_{\text{LZ}}$  has the following form,<sup>16,18</sup>

$$H_{\text{LZ}} = \mu_B [g_e \mathbf{B} \cdot \mathbf{S}_e + K \mathbf{B} \cdot \mathbf{J}_h + L (J_x^3 B_x + J_y^3 B_y + J_z^3 B_z)], \quad (6)$$

while the quadratic Zeeman term is represented by

$$H_{\text{QZ}} = c_1 B^2 + C_2 (\mathbf{J}_h \cdot \mathbf{B})^2 + C_3 [\frac{1}{2} B_x B_y (J_{hx} J_{hy} + J_{hy} J_{hx}) + \text{c.p.}], \quad (7)$$

where c.p. denotes cyclic permutations.<sup>19</sup> In these expressions  $\mathbf{S}_e$  and  $\mathbf{J}_h$  are the total angular momenta of the bound electron and bound hole, respectively.  $\mu_B$  is the Bohr magneton and  $x, y, z$  refer to the usual cubic axes.

### C. The perturbation matrix and the bound exciton wave functions

The standard method of obtaining the eigenfunctions and eigenenergies for the BE states, related to the perturbation Hamiltonian described above, is to apply perturbation theory on a set of unperturbed BE eigenstates. These unperturbed eigenstates may be defined in two different ways, either as the set of  $|m_e, m_h\rangle$  BE wave

functions, where  $|m_e, m_h\rangle$  is the product wave function of the individual unperturbed electron and hole wave functions  $|m_e\rangle = |S_e, m_e\rangle$  and  $|m_h\rangle = |J_h, m_h\rangle$ , respectively, or as the set  $|J, M\rangle$ , where  $J = J_h + S_e$ , appropriate for an exchange-coupled  $e$ - $h$  pair (BE).<sup>20</sup> The set  $|J, M\rangle$  diagonalizes the isotropic  $e$ - $h$  exchange interaction, removing the degeneracy of the  $J = 1$  and  $J = 2$  BE states in tetrahedral symmetry. The two sets of BE eigenstates are related by a simple unitary transformation  $|J, M\rangle = T^{-1} |m_e, m_h\rangle$ . In the treatment below, the  $|m_e, m_h\rangle$  basis set will be used for the unperturbed BE states.

The perturbed eigenenergies are obtained from the secular equation

$$\det \| H_{ij}^{\text{BE}} - E^i \delta_{ij} \| = 0, \quad (8)$$

where  $H_{ij}^{\text{BE}} = \langle \phi_i | H^{\text{BE}} | \phi_j \rangle$ , with  $H^{\text{BE}}$  according to Eq. (4) ( $B = 0$ ) or Eq. (5) ( $B \neq 0$ ), and  $\phi_i$  ( $i = 1-8$ ) are the eight unperturbed BE wave functions. In this diagonalization procedure the perturbed BE eigenfunctions are also obtained, as linear combinations of the unperturbed ones. Without external field the matrix  $H_{ij}^{\text{BE}}$  in Eq. (8) takes the following explicit form using the  $|m_h, m_e\rangle$  basis set [see Eq. (9)].

Performing the above diagonalization (again for zero field), the following explicit results are obtained for the energies of the eight perturbed BE eigenstates:

$$\begin{aligned} E_1 &= \frac{a}{4} + [(a+D)^2 + 3E^2]^{1/2}, \\ E_2 &= \frac{a}{4} - [(a+D)^2 + 3E^2]^{1/2}, \\ E_3 &= -\frac{3}{4}a + (D^2 + 3E^2)^{1/2}, \\ E_4 &= -\frac{3}{4}a - (D^2 + 3E^2)^{1/2}, \\ E_{5,6} &= \frac{a}{4} + (D^2 - aD + a^2 + 3E^2 \pm 3aE)^{1/2}, \\ E_{7,8} &= \frac{a}{4} - (D^2 - aD + a^2 + 3E^2 \pm 3aE)^{1/2}. \end{aligned} \quad (10)$$

This solution can be graphically illustrated for different values of the local-field parameters  $D$  and  $E$ , relative to the value of  $a$ . Such a representation is shown in Fig. 1, where the development of level splittings for three values of  $E/a$  ranging from 0 to 0.154 is shown, values typical for NN pairs in GaP (see below). It is evident that the  $E$  term already at quite low strength has a strong influence on the energy-level splitting of the BE states, particularly when the  $D$  parameter is small.

#### D. Relative oscillator strengths of the zero-field BE lines

The diagonalization of the matrix in Eq. (9) also gives the perturbed eigenfunctions for the BE states. These are now mixed relative to the unperturbed ones,<sup>20</sup> due to the crystal field at the defect. This means that the oscillator strengths of the BE lines are also changed. The relative oscillator strengths among the split BE states can be

$$\begin{array}{c} \left. \begin{array}{l} | \frac{3}{2}, -\frac{3}{2} \rangle | \frac{1}{2}, -\frac{1}{2} \rangle \\ | \frac{3}{2}, -\frac{1}{2} \rangle | \frac{1}{2}, -\frac{1}{2} \rangle \\ | \frac{3}{2}, \frac{1}{2} \rangle | \frac{1}{2}, -\frac{1}{2} \rangle \\ | \frac{3}{2}, \frac{3}{2} \rangle | \frac{1}{2}, -\frac{1}{2} \rangle \\ | \frac{3}{2}, -\frac{3}{2} \rangle | \frac{1}{2}, \frac{1}{2} \rangle \\ | \frac{3}{2}, -\frac{1}{2} \rangle | \frac{1}{2}, \frac{1}{2} \rangle \\ | \frac{3}{2}, \frac{1}{2} \rangle | \frac{1}{2}, \frac{1}{2} \rangle \\ | \frac{3}{2}, \frac{3}{2} \rangle | \frac{1}{2}, \frac{1}{2} \rangle \end{array} \right\} \begin{array}{c} | \frac{3}{2}, -\frac{3}{2} \rangle | \frac{1}{2}, -\frac{1}{2} \rangle \\ | \frac{3}{2}, -\frac{1}{2} \rangle | \frac{1}{2}, -\frac{1}{2} \rangle \\ | \frac{3}{2}, \frac{1}{2} \rangle | \frac{1}{2}, -\frac{1}{2} \rangle \\ | \frac{3}{2}, \frac{3}{2} \rangle | \frac{1}{2}, -\frac{1}{2} \rangle \\ | \frac{3}{2}, -\frac{3}{2} \rangle | \frac{1}{2}, \frac{1}{2} \rangle \\ | \frac{3}{2}, -\frac{1}{2} \rangle | \frac{1}{2}, \frac{1}{2} \rangle \\ | \frac{3}{2}, \frac{1}{2} \rangle | \frac{1}{2}, \frac{1}{2} \rangle \\ | \frac{3}{2}, \frac{3}{2} \rangle | \frac{1}{2}, \frac{1}{2} \rangle \end{array} \end{array} \quad (9)$$

$$\begin{array}{cccccccc} -\frac{3}{4}a - D & 0 & 0 & 0 & 0 & 0 & 0 & 0 \\ 0 & -\frac{a}{4} + D & 0 & \sqrt{3}E & 0 & 0 & 0 & 0 \\ \sqrt{3}E & 0 & \frac{a}{4} + D & 0 & 0 & 0 & 0 & 0 \\ 0 & \sqrt{3}E & 0 & 0 & \sqrt{3}E & -\frac{\sqrt{3}}{2}a & 0 & 0 \\ 0 & 0 & 0 & 0 & 0 & 0 & 0 & 0 \\ 0 & 0 & 0 & 0 & 0 & 0 & 0 & 0 \\ 0 & 0 & 0 & 0 & 0 & 0 & 0 & 0 \\ 0 & 0 & 0 & 0 & 0 & 0 & 0 & 0 \end{array}$$

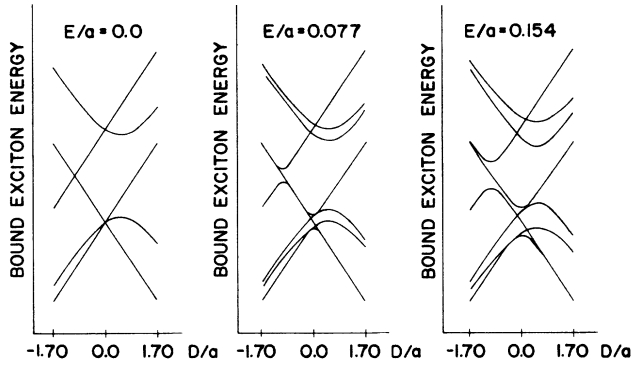


FIG. 1. The splitting of bound-exciton substates for an exchange-coupled pair with the basic states  $J=1$  and  $J=2$  without local field. The influence of the local-field parameters  $D$  and  $E$  is illustrated for  $-1.70 < D/a < +1.70$ , and for three different values of  $E/a$ . The exchange splitting between the "unperturbed"  $J=2$  and  $J=1$  states equals  $2a$ .

computed from the transition probabilities  $|\mathbf{M}_{e_i,g}^{\text{BE}}|^2$ , where

$$\mathbf{M}_{e_i,g}^{\text{BE}} = \langle \phi_{e_i}^{\text{BE}} | \mathbf{Q} | \phi_g^{\text{BE}} \rangle. \quad (11)$$

Here,  $\mathbf{Q}$  is the electric dipole moment operator,  $\phi_{e_i}^{\text{BE}}$  is the perturbed wave function of the BE states ( $i=1-8$ ), and  $\phi_g^{\text{BE}}$  is the ground state (with no particle) of the BE. Knowing the perturbed wave functions, which are functions of the parameters  $D$ ,  $E$ , and  $a$ , in the zero-field case, the relative oscillator strengths can be computed for any value of  $a$ ,  $D$ , and  $E$ , and compared with experimental data from absorption or PLE spectra. Figure 2 shows some examples of computed relative oscillator strengths (using a VAX 11/780 computer) for various values of the different parameters  $a$ ,  $D$ , and  $E$ . In cases where  $J$  (the total angular momentum for the BE) is a good quantum number, the transition from  $J=1$  to  $J=0$  (ground state) is dipole allowed, while the corresponding transition from  $J=2$  is forbidden. This means that when  $E=D=0$ , only the  $J=1$  state is ideally observed in absorption [Fig. 2(a)]. (Phonon coupling may mix these states slightly, to make the  $J=2$  state observable, but these effects are neglected in the present discussion.) In the case where  $D \neq 0$ , but  $E=0$  ( $C_{3v}$ ), the  $D$  term mixes the substates " $m_J = \pm 1$ " (" $J=1$ ") and " $m_J = \pm 1$ " (" $J=2$ "). Also, there is a splitting between  $m_J=0$  and  $m_J = \pm 1$  for " $J=1$ " and between  $m_J = \pm 1$  and  $m_J=2$  for " $J=2$ ." ( $J$  is no longer a good quantum number in this symmetry.) Three allowed lines may then be seen in absorption; their relative oscillator strengths depend on the ratio  $D/a$  [Figs. 2(b) and 2(c)]. In Fig. 3 we show the relative oscillator strength between the " $m = \pm 1$ " (" $J=2$ ") and " $m_J = \pm 1$ " (" $J=1$ ") transitions as a function of the ratio  $D/a$  in this case. In the case where both  $D$  and  $E$  are nonzero (symmetry lower than  $C_{3v}$ ), all eight lines may be observed, separated in energy, but some of them may be quite weak [Fig. 2(d)], depending on the relative values on  $D$ ,  $E$ , and  $a$ . As a comparison, in Fig. 2(e) we show a cor-

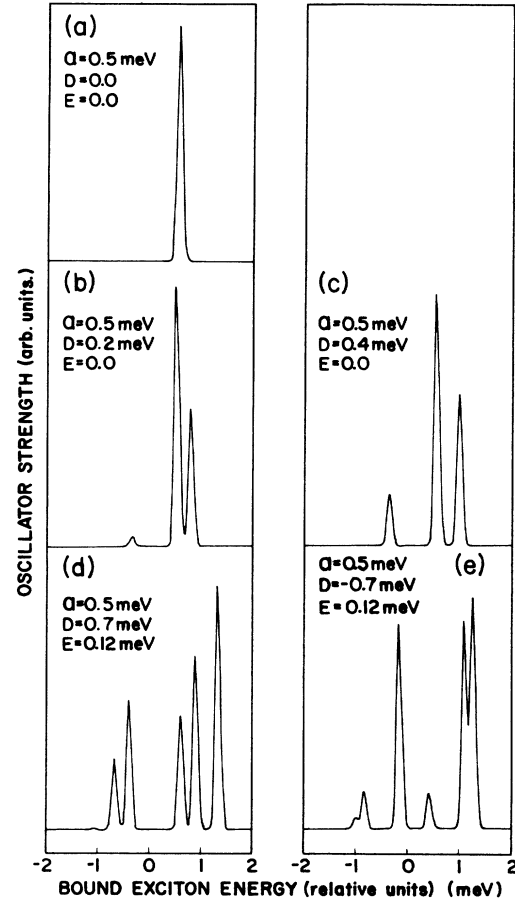


FIG. 2. Theoretically simulated spectra (relative oscillator strengths) for the BE system for the different values of the parameters  $a$ ,  $D$ , and  $E$  shown in each case.

responding spectrum with the same value of  $a$ ,  $E$ , and  $D$ , but with a negative sign of  $D$ .

In a similar way oscillator strengths can be computed, when the magnetic field is not zero, using the full Hamiltonian of Eq. (6).

#### IV. EXPERIMENTAL RESULTS FOR ZERO FIELD

PLE spectra have been published previously for NN pairs in GaP,<sup>5</sup> but no absorption results have been given

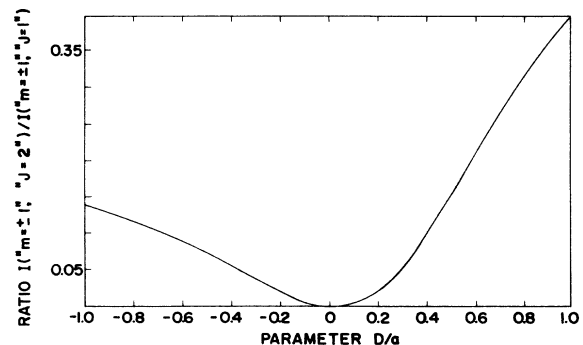


FIG. 3. Calculated ratio between the oscillator strengths of the substates " $m = \pm 1$ " (" $J=2$ ") and " $m = \pm 1$ " (" $J=1$ ") vs  $D/a$ , relevant for trigonal symmetry ( $C_{3v}$ ).

for the weaker components of the BE lines. These occur at lower energies than the strong “ $J=1$ ”-related lines and are always much weaker in absorption compared to the strong lines. It is therefore not possible to detect the weak components by straightforward transmission experiments on epitaxial layers, since such layers are usually too thin. In the previous PLE studies for the single-particle excited states,<sup>5</sup> epitaxial layers could not be used. Nevertheless, it was possible in this work, by carefully optimizing the experimental conditions, to obtain PLE spectra for the electronic lines of some NN-pair BE systems, including also the weak lines. An example is shown in Fig. 4(a), for the NN<sub>1</sub> BE. The PL spectrum is shown as a comparison (Fig. 5); here the weak lines appear much stronger due to thermalization. From the PLE spectrum in Fig. 4(a), the relative oscillator strengths of the weak lines can be deduced, as well as those for the strong lines.

The fit of the experimental PL spectrum to the expression in Eq. (10) gives explicit results for  $a$ ,  $D$ , and  $E$ , as shown in Table I. A critical test of this result is the calculation of oscillator strengths with the corresponding perturbed BE wave functions, according to Eq. (11) [Fig. 4(b)]. Allowing for the observed variation in broadening of the experimental peaks, the agreement between com-

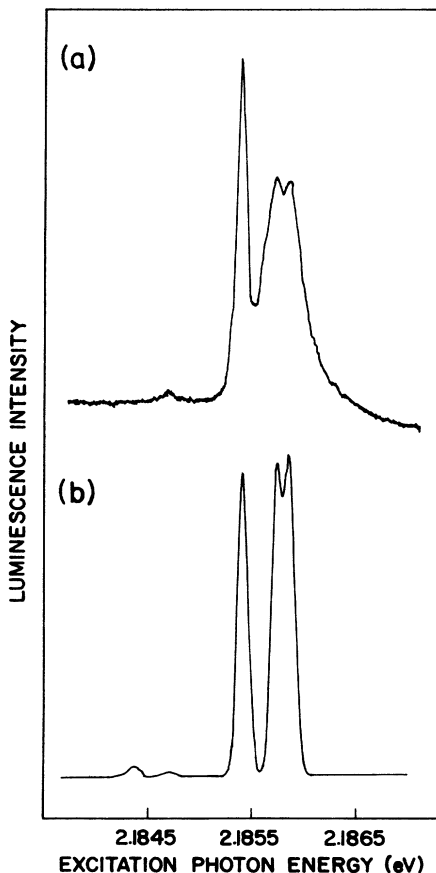


FIG. 4. (a) Photoluminescence excitation (PLE) spectrum for the NN<sub>1</sub> emission, measured with scanning dye-laser excitation at 4.2 K. The detection is set at the LO-phonon replica of the NN<sub>1</sub> lines. (b) A theoretically simulated spectrum for NN<sub>1</sub>, with the parameters listed in Table I.

TABLE I. A synopsis of the parameters in the perturbation Hamiltonian describing the Zeeman splitting of the NN<sub>1</sub>-pair bound exciton in GaP:N.

Parameters (NN <sub>1</sub> line)
$a = 0.585 \pm 0.005$ meV
$D = 0.20 \pm 0.01$ meV
$E = 0.095 \pm 0.005$ meV
$g_e = 1.85 \pm 0.05$
$K = 1.21 \pm 0.01$
$L = -0.05 \pm 0.01$
$C_1 = C_2 = C_3 = 0$

puted and observed oscillator strengths for the NN<sub>1</sub> BE is rather good, given the rather simple assumptions on the BE wave functions.<sup>20</sup> The observed ratio between the oscillator strengths of the weak “ $J=2$ ” components and the stronger “ $J=1$ ” lines is about 0.014 from Fig. 4(a), as compared to about 0.01 for the isolated  $N_p$  BE.<sup>1</sup>

An interesting observation in the PLE spectrum of Fig. 4(a) is the fact that the two strong lines observed at highest energy are much broader than the lowest line in the “ $J=1$ ” multiplet. We believe one reason for this broadening is an interaction with a background of low-energy phonons coupling to the lowest allowed line. It should also be noted that the simplified basis set used here for the BE wave functions neglects possible differences in the spatial part of the wave functions of the different substates. The wave functions used are apparently quite good for the calculation of transition energies, but may be less accurate for the oscillator strengths. A first-principles many-band calculation of the wave functions for the BE states of NN pairs does not exist (this is a difficult problem even for a single-particle state).

## V. EXPERIMENTAL ZEEMAN DATA

Figure 5 shows the zero-field spectrum of the NN<sub>1</sub> BE at 4.2 K, where all the BE lines are resolved, due to thermalization. Already from this spectrum it is obvious that the natural linewidth is an important parameter, determining the accuracy of the determined energy positions of the BE lines, which in this case are partly overlapping.

In a magnetic field the zero-field pattern in Fig. 5 develops into a fan diagram (Fig. 6), showing the splitting with magnetic field of each nonequivalent set of defects, with the particular direction chosen for the magnetic field [in this case  $\mathbf{B}$  5° off the  $K$  axis (Fig. 8)]. An example of a PL spectrum at 6 T is shown in Fig. 5. With the spectral linewidths given for these samples, some overlap between different lines is inevitable.

Figure 7 shows an angular dependence of the Zeeman spectrum for the NN<sub>1</sub> BE, rotating the sample with  $\mathbf{B}$  in the  $KK'$  plane (see Fig. 8). It is noted that the anisotropy observed in this diagram is not large. This anisotropy is derived mainly from the local-crystal-field and/or the Zeeman terms. Clearly, a very delicate comparison of a Hamiltonian with the data is necessary to determine the

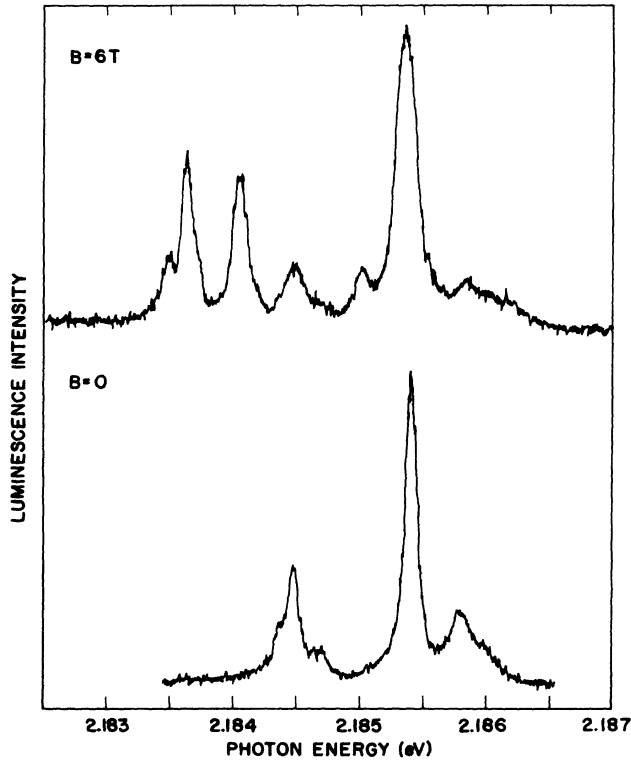


FIG. 5. Photoluminescence spectra of the zero-phonon part of the  $NN_1$  bound exciton, measured with  $Ar^+$ -ion laser excitation ( $5154 \text{ \AA}$ ) at 4.2 K. Spectra are shown both for zero field (bottom) and for a magnetic field of  $B = 6 \text{ T}$  (top).

physical parameters from these Zeeman data.

The low-symmetry plane used for the rotation of the sample was not chosen by design, but simply due to misalignment of the sample during the mounting procedure. It was difficult to achieve accurate alignment of the sample with  $B$  in a high-symmetry plane. Such an alignment would have facilitated a rough evaluation of

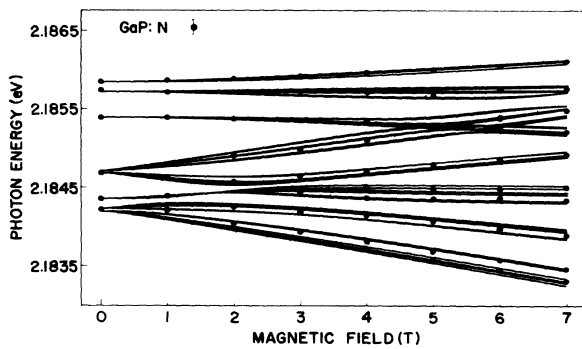


FIG. 6. Fan diagram for the splitting of the  $NN_1$  bound-exciton line with magnetic field, varying from  $B = 0 \text{ T}$  to  $B = 7 \text{ T}$ . The solid lines are computer simulated from the spin Hamiltonian given in the text with the parameters given in Table I [Eq. (5)], while the solid points correspond to resolved experimental lines. The linewidth of the broadest experimental lines is indicated by the error bar at the top.

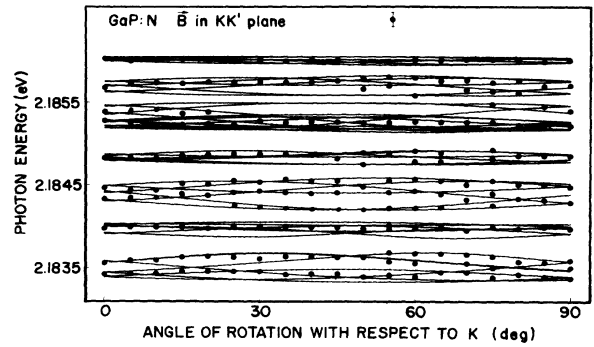


FIG. 7. Angular dependence of the Zeeman splitting of the  $NN_1$  bound-exciton lines, obtained in the Voigt configuration at 4.2 K. The sample was misoriented from the (110) plane, and the plane of rotation of the magnetic field  $B$  was the plane  $KK'$ , as defined separately in Fig. 8. The solid lines are computer simulated from the spin Hamiltonian given in the text [Eq. (5)], with the parameters given in Table I. Experimental lines are represented by solid points, the linewidth of the broadest lines is indicated by the error bar at the top.

data merely by inspection. To get an accurate evaluation it is necessary to determine the orientation precisely, which was done after the Zeeman measurements in this case, with the sample still mounted on the sample holder. Since the computer program used in the fitting of the data was flexible enough to allow analysis with an arbitrary plane of rotation, the alignment procedure did not

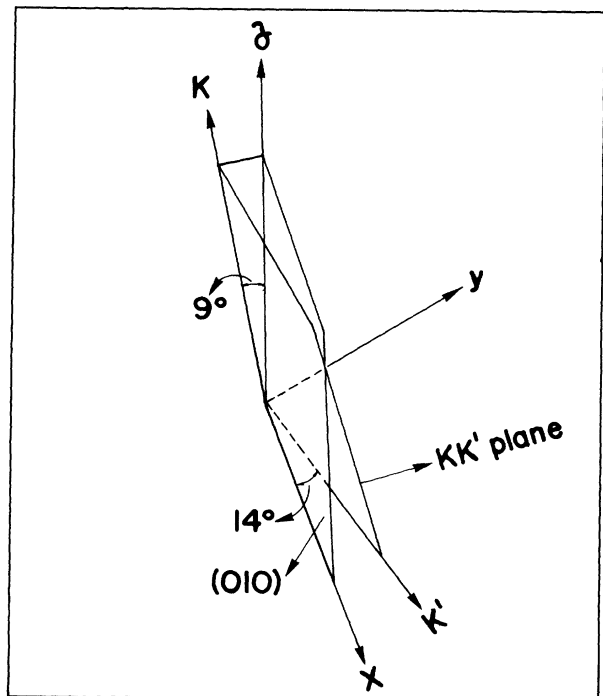


FIG. 8. This figure defines the plane of rotation of the magnetic field  $B$  for the data in Fig. 7.  $B$  was rotated in the  $KK'$  plane, and the angle of rotation was defined with respect to the  $K$  axis.

influence the accuracy of the evaluated parameters.

The Hamiltonian  $H^{\text{BE}}$  from Eqs. (4)–(6) above was used in the fitting to the experimental Zeeman data, in a similar way as described in Ref. 16. For the unperturbed BE states the basis set  $|m_e, m_h\rangle$  was used,<sup>20</sup> i.e., eight BE basis functions, sufficient for shallow effective-mass-like hole states.<sup>16</sup> The perturbed eigenenergies were obtained from the secular equation [Eq. (8)] as described above.

The eigenenergies  $E_i$  for each perturbed BE state are computed from Eq. (5) (with a VAX 11/780 computer) at any value of magnetic field and angle of rotation, with a program automatically producing a least-squares fit to the data. This procedure produces the simulated theoretical spectra shown as solid lines in Figs. 6 and 7, where the inequivalent sets of defects with respect to the magnetic field give different energies at nonzero magnetic field. The evaluated parameters for best fit in Figs. 6 and 7 are given in Table I for the  $\text{NN}_1$  BE.

## VI. DISCUSSION

This paper contains novel experimental PLE data on the relative oscillator strengths of the electronic BE lines associated with the  $\text{NN}_1$  pair. The perturbation Hamiltonian has been defined in somewhat more convenient notation than in Ref. 7, and also the basis set describing the unperturbed BE wave function is chosen as  $|m_e, m_h\rangle$ , which makes the secular matrix equation [Eq. (8)] simpler than the corresponding Eq. (10) of Ref. 7. The eigenenergies are given explicitly for the eight sublevels relevant for  $C_{2v}$  symmetry, in terms of the strain parameters  $D$  and  $E$ . This is an improvement compared to Ref. 7, where the  $E$  term was treated by perturbation theory, so that no explicit solutions were deduced in this symmetry. The computed dependence of level splitting on the relative strength of the  $E$  parameter differs drastically from the results in Fig. 7 in Ref. 7, obtained by a perturbation approach for  $E$  (denoted  $\varepsilon_2$  in Ref. 7). As a consequence, also the deduced  $E$  value for  $\text{NN}_1$  in our analysis is quite different, but more accurate (we find  $E=0.095$ , while in Ref. 7 a value  $\varepsilon_2=0.26$  is given). Our  $D$  value ( $D=0.20$ ) is also smaller than the value  $\varepsilon_1=0.3$  derived in Ref. 7. The  $a$  value is slightly larger than previously deduced (a value  $\gamma=2a=1.0$  meV is given in Ref. 7; we find  $2a=1.19$  meV).

The new values of  $D$  and  $E$  parameters presented in this work seem to be consistent with what might be expected for a bound exciton associated with substitutional pair defect. In this case the  $D$  value should dominate over  $E$ , since both impurity atoms are the same, and the axial part of the crystal field would then be expected to dominate over the  $E$  term, which mainly reflects the (smaller) disturbance of the surrounding atoms. The positive value of  $D$  is consistent with a local strain field of a tensional sign, which is indeed expected if two smaller atoms (N) are replacing the larger P atoms in the GaP lattice. In fact, this sign of  $D$  turns out to be quite common for substitutional pair defects also in other semiconductors.<sup>21–23</sup>

Previous PLE data for single-particle excited hole

states for the NN BE's have convincingly shown that the hole is bound as a secondary shallow-acceptor-like particle, in the low-symmetry crystal field of the defect.<sup>5</sup> Due to the delocalized character of the bound hole, the effect of the crystal field is rather small, even compared to the  $e$ - $h$  exchange splitting ( $=2a$ ; see Table I), which is around 1 meV for BE's associated with isolated  $N_p$  and NN pairs.<sup>1,3</sup> Therefore the electronic structure can approximately be discussed in terms of Fig. 9, where the assumption of  $J_h = \frac{3}{2}$  hole states already discussed above is used to develop the basic exchange-split states " $J=1$ " and " $J=2$ ," which further split in a local crystal field of tensional sign, as shown in the right-hand part of Fig. 9. The resulting zero-field-splitting pattern should be directly compared with the zero-field energies in Figs. 4 and 5.

The zero-field oscillator strengths expected for the BE lines from the simple model of a BE wave function as a simple direct product of a spinlike electron and a  $p$ -like hole were computed in this work for the first time, using the BE eigenfunctions resulting from the diagonalization of the perturbation matrix equation. Although computing such oscillator strengths is a quite sensitive way of testing the accuracy of wave functions, the results for  $\text{NN}_1$  are in good agreement with experimental data in spite of the simple basis set used for the BE wave function.<sup>20</sup> This is a support for the simple physical model for the BE (the HTL model<sup>17</sup>) with a delocalized effective-mass-like shallow hole state, as also confirmed by the Zeeman data reported in this work.

Since the electronic BE wave functions are deduced from simplified assumptions on the electronic structure, they must be regarded as only approximate. Therefore the fitting of the zero-field spectrum without Zeeman data may not be unique, particularly when the effects of

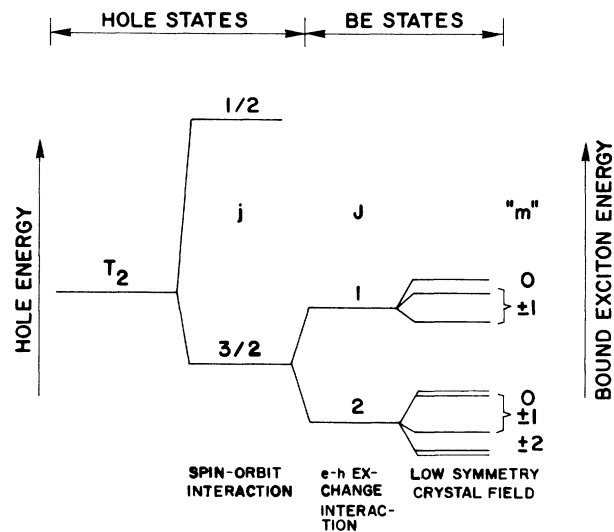


FIG. 9. Schematic perturbative representation of the electronic structure for the NN bound excitons in GaP:N. The electron-hole exchange interaction dominates, but the effects of the local strain field are of the same order, so that a low-symmetry strain field may cause observable splittings of all degeneracies.

the local field are weak, and some of the lines are nearly degenerate and not separately resolved. The development of each particular BE line with magnetic field is then an additional powerful means of verifying the BE level structure at zero field. This could be done in this work for the  $NN_1$  defect.

An important piece of information which is obtained from the Zeeman data is the symmetry of the defect. Already the appearance of the zero-field spectrum can only be conveniently fitted with  $C_{2v}$  symmetry, as noted above. A powerful procedure is the fitting of the angular dependence and fan diagram (Figs. 6 and 7), accounting for the independent information obtained from fitting the zero-field oscillator strengths. This way, the  $C_{2v}$  symmetry for the  $NN_1$  pair was firmly concluded, i.e., a nearest-neighbor [110]-oriented substitutional pair at P sites, as independently concluded from recent uniaxial stress data.<sup>9</sup>

The Zeeman Hamiltonian in this work is the standard one used for a complex defect in tetrahedral symmetry, when the electrons are spinlike and the holes  $p$ -like ( $\Gamma_8$ ), as is appropriate in the Hopfield-Thomas-Lynch (HTL) model<sup>17</sup> for a delocalized effective-mass-like hole.<sup>19</sup> The isotropic  $g$  value  $K$  is not so much different from, but slightly larger than what is usually found for shallow hole states in GaP, i.e., the hole in the BE bound to shallow substitutional donors.<sup>4,24</sup> The anisotropy parameter is also quite small, as may be expected for a quite delocalized hole state. The obtained values justify the use of a simple linear Zeeman Hamiltonian in this case.

The  $g$  value for the electron,  $g_e$ , is found to be  $g_e = 1.85$ , which is reduced from the value  $g_e \approx 2.00$  found for most shallow donors in GaP,<sup>25,26</sup> but also the value 2.00 expected for a very strongly localized spinlike electron.<sup>16</sup> A small negative  $g$  shift is typical for shallow donor states due to a small spin-orbit-induced perturbation.<sup>27</sup> For this N-related BE the electron wave function is supposed to be dominated by a strongly localized part, but the detailed wave function is not known, and should be computed by deep-level theory. Therefore, at present, it does not seem possible to theoretically predict any  $g_e$  value for comparison with the experimental one. It should be noted that the  $g_e$  values previously derived for the electron bound in the isolated  $N_p$  BE vary between  $g_e = 2.02 \pm 0.12$  (Ref. 28) and  $g_e = 1.96 \pm 0.03$  (Ref. 29). For the slightly deeper but likewise electron-attractive Li-Li-O defect in GaP, a slightly reduced  $g$  value,  $g_e = 1.76 \pm 0.14$ , has been reported,<sup>30</sup> i.e., similar to the

value for the  $NN_1$  BE obtained in this work.

An interesting observation in the  $NN_1$  BE Zeeman data is the absence of quadratic shifts of the BE lines. This is perfectly consistent with the notion that the bound electron is quite localized, and non-effective-mass-like. Strong quadratic shifts of BE lines are typically observed only for delocalized electron states, such as shallow donor electrons or electrons bound as a secondary particle in BE's.<sup>31</sup>

## VII. CONCLUSIONS

In this work we present novel experimental data for the  $NN_1$  pair defect in GaP, notably PLE spectra for the substructure of the electronic lines, revealing the relative oscillator strengths, and, in addition, the Zeeman data for magnetic fields up to 7 T. A more detailed analysis of the zero-field spectra than previously available has been developed, giving explicit expressions for the energies of all substates in  $C_{2v}$  symmetry, as a function of the local-field parameters  $D$  and  $E$  and the exchange parameter  $a$ . In addition, oscillator strengths have been computed for the BE substates as a function of the same parameters, which appears to be quite valuable for the detailed assignment of the different BE substates.

The Zeeman data combined with the computed zero-field energy spectra and oscillator strengths allow the firm conclusion of a  $C_{2v}$  symmetry for the  $NN_1$  defect, consistent with an identity as a nearest-neighbor substitutional pair on P sites along the [110] direction. The obtained  $g$  values for the electron and hole are consistent with the Thomas-Hopfield-Lynch BE model with a quite localized electron and a shallow delocalized hole. The electron-hole exchange splitting  $2a = 1.19$  meV is slightly larger than that for the isolated  $N_p$  BE, as expected due to a slightly more localized hole state for  $NN_1$ . The values for  $D$  and  $E$  are substantially smaller than previously deduced from an approximate evaluation of photoluminescence data.

## ACKNOWLEDGMENTS

We are grateful to A. R. Peaker of University of Manchester and M. Yamanaka of Showa Denko KK, Japan, for supplying the N-doped epitaxial GaP material used in this work. In addition, we acknowledge fruitful conversations with W. M. Chen and P. O. Holtz.

<sup>1</sup>D. G. Thomas and J. J. Hopfield, Phys. Rev. **150**, 680 (1966).

<sup>2</sup>J. J. Hopfield, P. J. Dean, and D. G. Thomas, Phys. Rev. **158**, 748 (1967).

<sup>3</sup>J. L. Merz, A. Baldereschi, and A. M. Sergent, Phys. Rev. B **6**, 3082 (1972).

<sup>4</sup>P. J. Dean and D. C. Herbert, *Excitons*, Vol. 14 of *Topics in Current Physics*, edited by K. Cho (Springer, Berlin, 1979), pp. 55–182.

<sup>5</sup>E. Cohen and M. D. Sturge, Phys. Rev. B **15**, 1039 (1977).

<sup>6</sup>H. Mathieu, P. Merle, L. Bayo, and J. Camassel, Phys. Rev. B **22**, 4710 (1980).

<sup>7</sup>B. Gil, J. Camassel, P. Merle, and H. Mathieu, Phys. Rev. B **25**, 3987 (1982).

<sup>8</sup>B. Gil, M. Baj, J. Camassel, H. Mathieu, C. Benoit à la Guillaume, N. Mestres, and J. Pascual, Phys. Rev. B **29**, 3398 (1984).

<sup>9</sup>B. Gil, J. Camassel, J. P. Albert, and H. Mathieu, Phys. Rev. B **33**, 2690 (1986).

- <sup>10</sup>See, for example, *Light Emitting Diodes*, edited by A. A. Bergh and P. J. Dean (Oxford University Press, New York, 1976), p. 468.
- <sup>11</sup>R. A. Faulkner, *Phys. Rev.* **175**, 491 (1968).
- <sup>12</sup>J. C. Phillips, *Phys. Rev. Lett.* **22**, 285 (1968).
- <sup>13</sup>A. Baldereschi and J. J. Hopfield, *Phys. Rev. Lett.* **28**, 171 (1972).
- <sup>14</sup>A. Arfi, W. T. Masselink, and Y. C. Chiang, *Phys. Rev. B* **33**, 2401 (1986).
- <sup>15</sup>B. Gil, J. P. Albert, J. Camassel, H. Mathieu, and C. Benoit à la Guillaume, *Phys. Rev. B* **33**, 2701 (1986).
- <sup>16</sup>B. Monemar, U. Lindelfelt, and W. M. Chen, in Proceedings of the 2nd International Conference on Shallow Impurities, Trieste, 1986 [*Physica B+C* **146B**, 256 (1987)].
- <sup>17</sup>J. J. Hopfield, D. G. Thomas, and R. T. Lynch, *Phys. Rev. Lett.* **17**, 312 (1966).
- <sup>18</sup>A. Abragam and B. Bleaney, *Electron Paramagnetic Resonance of Transition Metal Ions* (Clarendon, Oxford, 1970), p. 664.
- <sup>19</sup>J. M. Luttinger, *Phys. Rev.* **102**, 1030 (1955).
- <sup>20</sup>J. van W. Morgan and T. N. Morgan, *Phys. Rev. B* **1**, 739 (1970).
- <sup>21</sup>Q. X. Zhao, B. Monemar, and P. O. Holtz, *Phys. Rev. B* **36**, 3351 (1987).
- <sup>22</sup>B. Monemar, H. P. Gislason, W. M. Chen, and Z. G. Wang, *Phys. Rev. B* **33**, 4424 (1985).
- <sup>23</sup>P. O. Holtz, Q. X. Zhao, and B. Monemar, *Phys. Rev. B* **36**, 5051 (1987).
- <sup>24</sup>P. J. Dean, D. Bimberg, and F. Mansfeld, *Phys. Rev. B* **15**, 3906 (1977).
- <sup>25</sup>F. Mehran, T. N. Morgan, R. S. Title, and S. E. Blum, *Phys. Rev. B* **6**, 3917 (1972).
- <sup>26</sup>M. Godlewski, W. M. Chen, and B. Monemar, *Phys. Rev. B* **33**, 8246 (1986).
- <sup>27</sup>See, e.g., A. M. Stoneham, *Theory of Defects in Solids* (Clarendon, Oxford, 1985), p. 449.
- <sup>28</sup>Y. Yafet and D. G. Thomas, *Phys. Rev.* **131**, 2405 (1963).
- <sup>29</sup>J. L. Merz, R. A. Faulkner, and P. J. Dean, *Phys. Rev.* **188**, 1228 (1969).
- <sup>30</sup>P. J. Dean, *Phys. Rev. B* **4**, 2596 (1971).
- <sup>31</sup>W. Schairer, D. Bimberg, W. Kottler, K. Cho, and M. Schmidt, *Phys. Rev. B* **13**, 3452 (1976).